Jin, M. and Chen, Q. 2015. "Improvement of fast fluid dynamics with a conservative semi-Lagrangian scheme," *International Journal of Numerical Methods for Heat and Fluid Flow*, 25(1), 2-18.

Improvement of Fast Fluid Dynamics with a Conservative Semi-Lagrangian Scheme

Mingang Jin[1], Qingyan Chen[1]
[1]School of Mechanical Engineering, Purdue University, West Lafayette, IN 47906, USA
Qingyan Chen (Corresponding Author)
Email: yanchen@purdue.edu
Phone: +1-765-496-7562
Fax: +1-765-494-0539

Abstract

Purpose: This paper is to develop a simple and efficient conservative semi-Lagrangian scheme for solving advection equation in Fast Fluid Dynamics (FFD), so FFD can provide fast indoor airflow simulations while preserving conservation for energy and species transport.

Design/methodology/approach: This study thus proposed a mass-fixing type conservative semi-Lagrangian scheme that redistributes global surplus/deficit on the advected field after performing the standard semi-Lagrangian advection. The redistribution weights were designed to preserve the properties of conservatives and monotonicity.

Findings: The effectiveness of the conservative semi-Lagrangian scheme was validated with several test cases, and the results show that the proposed scheme is indeed conservative with negligible impact on the accuracy of the standard solutions.Findings- Our numerical tests show that the proposed scheme was indeed conservative with negligible impact on the accuracy of the flow prediction.

Originality/value: The FFD with conservative semi-Lagrangian scheme can effectively enforce the energy and species conservation for indoor airflow and predict airflow distributions with reasonable accuracy.

Keywords: Fast fluid dynamics, Conservative semi-Lagrangian, Indoor airflow

1. Introduction

Fast airflow simulations are often required in the building industry. One example is that, in the initial design stage, a tool providing fast simulations of airflow in and around buildings can enable architects and engineers to evaluate various building design options or ventilation strategies within a tight project schedule. Another example is in the area of emergency management in buildings: in case of fire, fast airflow simulations can help rescuers make active smoke-control plans and efficient evacuation plans. In addition, the efficiency of integrated building airflow and energy-simulation tools can be improved by taking advantage of fast airflow simulations.

Fast fluid dynamics (FFD), a recently developed model that is able to perform detailed airflow simulations at a very fast speed (Zuo and Chen 2009), is a potential tool for performing fast airflow simulations. Initially designed for visualizing fluid flow in computer games (Stam 1999), FFD was adapted and improved for simulating airflows in buildings (Zuo and Chen 2010, Zuo et al. 2010). Rather than creating plausible visual effects for fluid flows, FFD for engineering applications in buildings should be validated to predict the primary characteristics of airflows and to provide airflow parameters such as temperature, velocity, and species concentration with acceptable accuracy. Jin et al. (2012 and 2013) validated the FFD for simulating indoor airflows and natural ventilation in buildings, and found that the FFD was capable of capturing major airflow features inside and around the buildings. Although FFD cannot predict airflow details as accurate as CFD tools, it is over 15 times faster than CFD tools when the same grid size and time step size were used.

Additionally, it is also important that FFD provide airflow simulations with conservation of mass, energy, and species concentration. Although FFD has solved the partial differential governing equations for flow based on the conservation law, the non-conservative semi-Lagrangian scheme (SL) (Robert 1981) used in FFD may not enforce the conservation. FFD adopts SL to solve the advection equation, because it is not subject to the traditional Courant–Friedrichs–Lewy (CFL) condition that severely limits the maximum time step size. However, the standard SL has a major disadvantage in that it cannot maintain conservation of the advection quantity (Staniforth and Côté 1991). Therefore, in order to obtain conservative airflow simulations, it is necessary to improve the SL used in FFD.

Many studies have been conducted to improve the standard SL and realize conservative advection. Through conservative remapping, the standard SL can become inherently conserving. Rančič (1992 and 1995) and Laprise and Plante (1995) developed mass-conservative SL algorithms that are based on a cell-integrated SL that employs a piecewise parabolic method. Lauritzen et al. (2010) proposed a conservative SL with a multi-tracer transport algorithm on the cubed sphere. Zerroukat et al. (2002 and 2005) also developed an inherently conserving and efficient semi-Lagrangian scheme that is based on the control volume approach, and used multiple sweeps of a one-dimensional conservative remapping algorithm. SL with conservative remapping is more mathematically grounded and inherently satisfies local and global mass conservation (Zerroukat 2010). However, multi-dimensional remapping can be relatively expensive because of the additional geometric computations required; therefore, most applications of this type of conservative scheme are limited to one- or two-dimensional problems.

As with conservative remapping, some researchers developed conservative SL through modification of the interpolation weights. Kaas (2008) introduced modified interpolation weights at the upstream departure points to form a conservative SL. Lentine et al. (2011) proposed a conservative limiter to the typical SL interpolation step and devised a second step of forward advection to develop the conservative SL. Although these approaches are much simpler than conservative remapping, they may encounter the difficulty of generating non-monotonic solutions.

Another approach is known as the mass-fixing method. Through the application of post correction to the solution of the standard SL, the mass-fixing conservative SL could efficiently restore global conservation. Priestley (1993) developed a quasi-conservative SL based on the blending of high-order and low-order solutions. Bermejo and Staniforth (1992) applied Lagrangian multipliers in post correction and developed a conservative quasi-monotone SL. Zerroukat et al. (2010) also developed a conservative SL based on a simple explicit smoothness-based correction and monotonicity filter. Despite its ad hoc nature, the mass-fixing scheme is popular because of its simplicity and the convenience of incorporating it within an existing SL.

Because computing speed is the primary concern of FFD, a conservative SL with the mass-fixing method would be a good alternative for implementation in FFD. However, as was noted above, mass-fixing methods require both low-order and high-order solutions, whereas only first-order SL is implemented in current FFD. Therefore, it is necessary to propose a mass-fixing method that requires only a low-order solution.

This paper thus presents a mass-fixing conservative SL depending on a first-order solution to improve the performance of FFD for providing conservative airflow simulations. The proposed scheme was further tested to evaluate its impact on the accuracy and conservativeness of FFD simulations.

2. Research method

2.1 Fast Fluid Dynamics

Like computational fluid dynamics, FFD simulates airflow by numerically solving a set of partial differential equations (1)-(3), which represent the conservation of mass, momentum, and transported scalars, respectively.

$$\frac{\partial U_i}{\partial x_i} = 0, \tag{1}$$

$$\frac{\partial U_i}{\partial t} + U_j \frac{\partial U_i}{\partial x_j} = -\frac{1}{\rho}\frac{\partial p}{\partial x_i} + \nu \frac{\partial^2 U_i}{\partial x_j \partial x_j} + \frac{1}{\rho} F_i, \tag{2}$$

$$\frac{\partial \Phi}{\partial t} + U_j \frac{\partial \Phi}{\partial x_j} = \Gamma \frac{\partial^2 \Phi}{\partial x_j \partial x_j} + S, \tag{3}$$

where i, j = 1, 2, 3. U_i is the i^{th} component of the velocity vector, p pressure, ρ density, F_i the i^{th} component of the body forces, ν the kinetic viscosity, Φ the scalar to be solved, Γ the transport coefficient, and S the source term. However, to achieve airflow simulations with high computational efficiency, FFD applied a time-splitting scheme (Ferziger and Perić 1999) to solve the partial equations sequentially. FFD first solves the momentum equation (2) in the following three steps:

$$\frac{U_i^* - U_i^n}{\Delta t} = -U_j^n \frac{\partial U_i^n}{\partial x_j}, \tag{4}$$

$$\frac{U_i^{**} - U_i^*}{\Delta t} = \nu \frac{\partial^2 U_i^{**}}{\partial x_j \partial x_j} + \frac{1}{\rho} F_i, \tag{5}$$

$$\frac{U_i^{n+1} - U_i^{**}}{\Delta t} = -\frac{1}{\rho}\frac{\partial p}{\partial x_i}, \tag{6}$$

where U^n and U^{n+1} represent the velocity at the previous and current time step, respectively. In each time step, FFD first solves the advection equation (4) using a semi-Lagrangian scheme to obtain the intermediate velocity U^*, and then the diffusion equation (5) is solved implicitly for the intermediate velocity U^{**}. To resolve the coupling of pressure and velocity, the pressure

projection (Chorin 1967) is conducted to enforce the velocity field in satisfying the continuity. By substituting equation (2) into equation (1), the following Poisson equation can be derived:

$$\frac{\partial^2 P}{\partial x_j \partial x_j} = \frac{\rho}{\Delta t}\frac{\partial U_j^{**}}{\partial x_j}. \tag{7}$$

By solving equation (7) for pressure, FFD updates the velocity field with equation (6) to obtain U^{n+1}. After obtaining the velocity field, FFD then likewise solves scalar transport equation (3) with a time-splitting scheme.

$$\frac{\Phi^* - \Phi^n}{\Delta t} = -U_j \frac{\partial \Phi^n}{\partial x_j}, \tag{8}$$

$$\frac{\Phi^{n+1} - \Phi^*}{\Delta t} = \Gamma \frac{\partial^2 \Phi^{n+1}}{\partial x_j \partial x_j} + S, \tag{9}$$

where Φ^n and Φ^{n+1} represent the scalar quantity at the previous and current time step, respectively. After solving the transport equation for scalars such as temperature and species concentrations, FFD advances to the next time step and continues the simulation.

2.2 Conservative semi-Lagrangian scheme

FFD solves advection equations (4) and (8) with a semi-Lagrangian scheme, which applies the Lagrangian advection on the Eulerian grid and can achieve enhanced stability at larger time steps. For example, the semi-Lagrangian solution of advection equation (8) can be expressed as:

$$\Phi^*(\vec{x}_a) = \Phi^n(\vec{x}_d) = \Phi^n(\vec{x}_a - \Delta t\vec{U}) = \sum_{k=k1,k2..kN} w_k \Phi^n(\vec{x}_k), \tag{10}$$

where $\Phi^*(\vec{x}_a)$ is Φ^* at downstream points $\vec{x}_a = (x_1, x_2, x_3)$, and $\Phi^n(\vec{x}_d)$ and $\Phi^n(\vec{x}_k)$ represent Φ^n at departure points $\vec{x}_d$ and locations $\vec{x}_k$ of the cells surrounding the departure points, respectively. As shown in Figure 1, the semi-Lagrangian scheme uses two steps to predict the scalar quantity at $\vec{x}_a$ after advection. First, the departure location of the point at $\vec{x}_a$ is predicted by tracing back along the backward trajectory. In FFD, the first-order trajectory is used so that the departure location can be expressed as $\vec{x}_a - \Delta t\vec{U}$. Next, the value of Φ at the departure location is estimated by interpolation from surrounding cells. In FFD, only linear interpolation is applied so that only the adjacent cells are used to predict the value of Φ at the departure location. Although linear interpolation induces considerable numerical diffusion, it can be regarded as a substitute for turbulence viscosity and would be helpful for FFD simulation of indoor airflows without turbulence models.

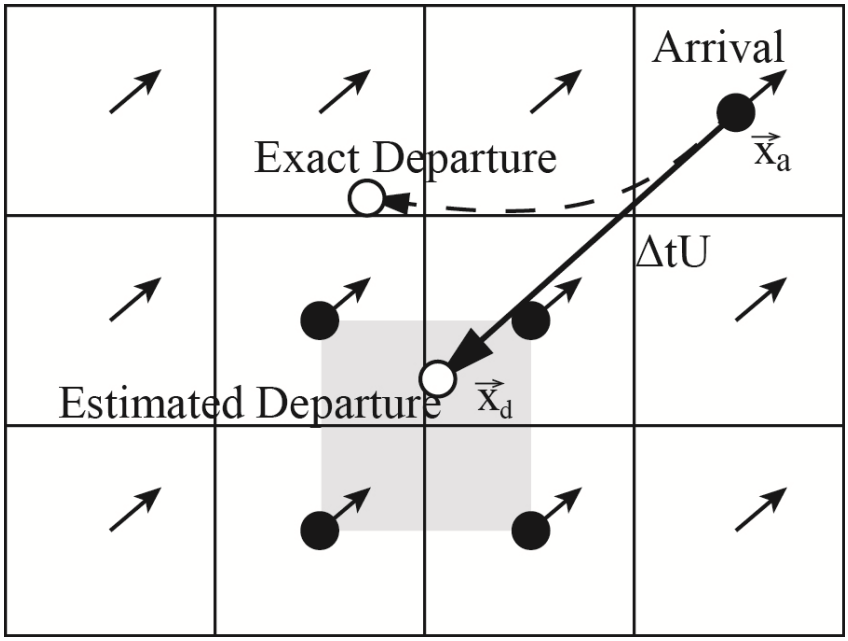

Figure 1 Illustration of the semi-Lagrangian scheme

However, as shown in Figure 1, the estimated backward trajectory might not be identical to the exact trajectory, particularly in FFD with a first-order SL. This error would cause inaccurate prediction of the departure position, so that each cell in the domain would not contribute evenly during advection; the result would be an unexpected loss or gain of the advection quantity of the scalar. Therefore, the use of a standard SL in FFD cannot ensure conservative advection. In addition, the interpolation errors would cause the standard SL to lose the property of conservation.

To enforce conservation during the advection process, this study proposed and implemented a mass-fixing conservative SL in FFD. Specifically, the standard SL advection was first performed on the scalar field, and then the deficit or surplus of the scalar quantity in the computation domain was computed. If $\widehat{\Phi}^*(\vec{x}_j)$ is the non-conservative solution obtained by the standard SL, then the global gain or loss of the scalar field can be expressed by β as:

$$\beta = \sum_{j=1}^{j=n} \Phi^n(\vec{x}_j) - \sum_{j=1}^{j=n} \widehat{\Phi}^*(\vec{x}_j) + \left(\sum\nolimits_{in} \Phi^n(\vec{x}_j) - \sum\nolimits_{out} \Phi^n(\vec{x}_j) \right), \tag{11}$$

where $\sum_{in} \Phi^n(\vec{x}_j)$ and $\sum_{out} \Phi^n(\vec{x}_j)$ are the scalar quantity transported into and out of the domain, respectively. A post correction was then performed by redistributing the deficit or surplus to the scalar field to restore the global conservation, using the following equation:

$$\Phi^*(\vec{x}_j) = \widehat{\Phi}^*(\vec{x}_j) + \eta_j \beta, \tag{12}$$

where η_j is the weighting factor determining the redistribution of the surplus or deficit. In addition, it is clear that advection can be conserved if equation (13) is satisfied:

$$\sum_{j=1}^{j=n} \eta_j = 1. \tag{13}$$

In principle, to satisfy the conservation, the choices for η_j can be arbitrary when equation (13) is valid. However, because the post correction is artificial, it should not have a significant influence on the solution derived by the standard SL. Therefore, the redistribution of the surplus or deficit to the scalar field should take into account the following solution properties similar as those proposed by Zerroukat (2010): (1) the correction should have little impact on the smooth part of the field; (2) the redistribution should not create overshoots or undershoots in the solution; and (3) the correction should be smooth rather than the on/off type. Therefore, this study proposed that the redistribution be proportional to the difference between the non-conservative solution and the local extremes around its departure positions. η_j can then be defined as follows.

If the original advection creates a deficit (β>0),

$$\eta_j = \frac{\left|\Phi^n(\vec{x}_d) - \Phi^+(\vec{x}_d)\right|}{\sum_{i=1}^{i=n}\left|\Phi^n(\vec{x}_i) - \Phi^+(\vec{x}_i)\right|}, \tag{14}$$

or if a surplus was created (β<0),

$$\eta_j = \frac{\left|\Phi^n(\vec{x}_d) - \Phi^-(\vec{x}_d)\right|}{\sum_{i=1}^{i=n}\left|\Phi^n(\vec{x}_i) - \Phi^-(\vec{x}_i)\right|}, \tag{15}$$

where $\Phi^+(\vec{x}_d)$ and $\Phi^-(\vec{x}_d)$ represent the local maximum and minimum values of the scalar quantity around the departure positions, respectively. It is clear that the distribution of weighting factors is continuous rather than the on/off type. In addition, the weighting factors are defined to avoid creating new local extremes after redistribution. If there a deficit is created, according to equation (14), it will be redistributed to the scalar field in such a manner that more is added to those cells which have a larger difference with the maximum value around its departure points. Therefore, the correction will not generate a local maximum as long as the deficit is small. Similarly, this scheme avoids creating a local minimum for redistributing the surplus. In addition, the weighting factors are small for smooth fields, so that the correction will have minimal impact on them. Therefore, the proposed correction method satisfies the afore-mentioned principles.

Because mass conservation is always enforced by the continuity equation, the conservative SL is applied in FFD only to solve the advection equations for transported scalars such as temperature and species concentration.

3. Results and discussion

As discussed in this section, the conservative SL was tested for four cases to assess its impact on the accuracy and conservativeness of the FFD simulations. The proposed conservative SL was first tested with a pure advection case. Next, its effects on energy and species conservation were examined separately. Finally, the improved FFD program was then applied to simulate airflows in an occupied office room with displacement ventilation, and its performance for predicting conservative indoor airflow simulations was evaluated. Please also note that this study did not perform grid dependence study for all the cases, as the results would be grid dependent with the

coarse grid used. The grid size was determined as designers would normally feel comfortable with the computing resources normally available in a designer's office. This investigation intentionally used coarser grid to achieve a faster computer speed in the FFD simulations as a designer would do, compared with CFD simulations.

3.1 Advection of a notched disk

A two-dimensional passive advection case was first used to test the performance of the conservative SL. In this case, a Zalesak disk (Zalesak 1979) was passively advected in a rotating velocity field. As shown in Figure 2, a disk with a notch was centered in the domain [0,100] × [0,100], with a uniform grid of size h = 0.5. The disk had a density of 1 and a radius of 15 h. The width and length of the notch were 5h and 25h, respectively. The background had a density of 0.

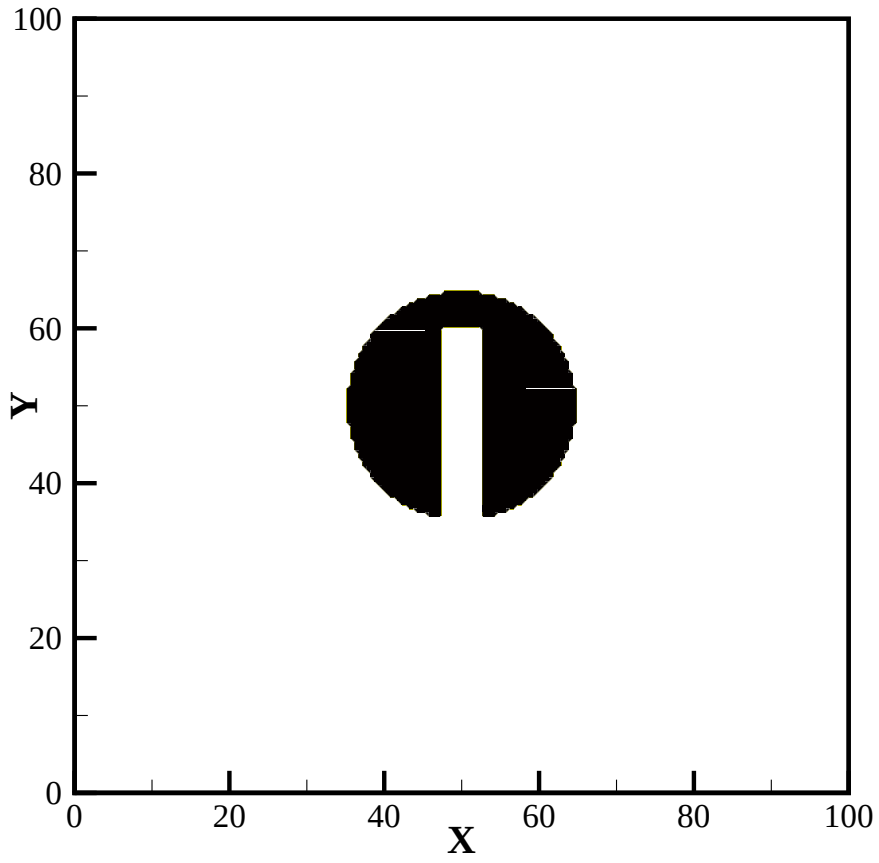

Figure 2. Schematic of the disk with a notch

The rotating velocity field can be specified by $u = (\pi / 5)(50 - y)$ and $v = (\pi / 5)(50 - x)$. This corresponds to one rotation every 10 s. With a time step size of 0.1 s, corresponding

maximum CFL number in the simulation is 3, a revolution is completed every 100 time steps. This study performed one revolution of the disk. The density profile across the center of the disk as predicted by standard and conservative SL was compared with the exact profile, as shown in Figure 3(a). Similar density profiles were predicted by these two schemes. Because both schemes adopted linear interpolation, the predicted profiles were too diffusive to preserve the shape of the disk well. Because of the post correction in the conservative SL, the mass was recovered for the disk and a wider density profile was predicted. Inspection of the density profile revealed that the regained mass was non-uniformly added to the non-conservative density profile predicted by the standard SL, as we expected. More mass was regained in those regions where discontinuity occurred, such as the disk edge and the narrow slot. As shown in Figure 3(b), with a larger time step size of 0.2s, the density profiles predicted by the standard SL shrunk further because of greater mass loss in the advection, whereas the conservative SL maintained the size of the density profile well. In addition, no overshoot or undershoot was found in the density profiles predicted by the conservative SL. Therefore, the proposed scheme can also preserve monotonicity.

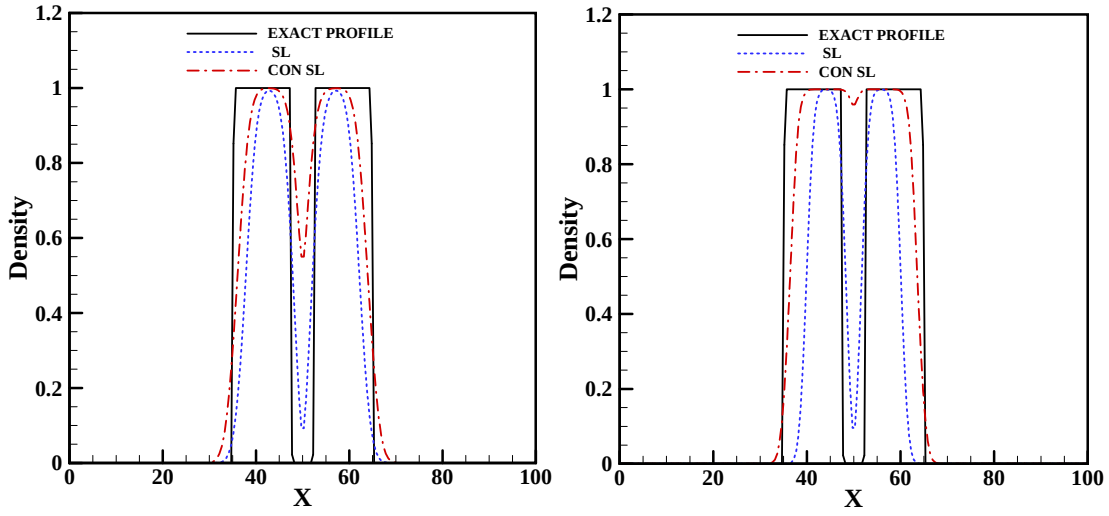

Figure 3. The density profile along the centerline of the disk after one rotation as predicted with time step sizes of (a) 0.1s and (b) 0.2s

Figure 4 shows the variation of the total mass of the disk during the revolution. After one rotation, significant mass loss was observed with the standard SL, but the conservative SL proved indeed to be conservative and maintained a constant total mass during the advection process with different step sizes. On the other hand, for the standard SL, greater mass loss can be observed with a larger time step size. In such a rotating velocity field, the predicted backward trajectory with first-order accuracy would generate greater error with a larger time step size, which would cause a more deviated departure point as compared to the exact one. With an inaccurately predicted departure point, each cell in the domain would contribute unevenly to the advected field. In this case, the background field with zero density contributed more than the disk in each advection step, so that the total mass diminished continuously as the advection continued. The background, in particular, would contribute even more with a larger time step size, so that a greater mass deficit would be generated.

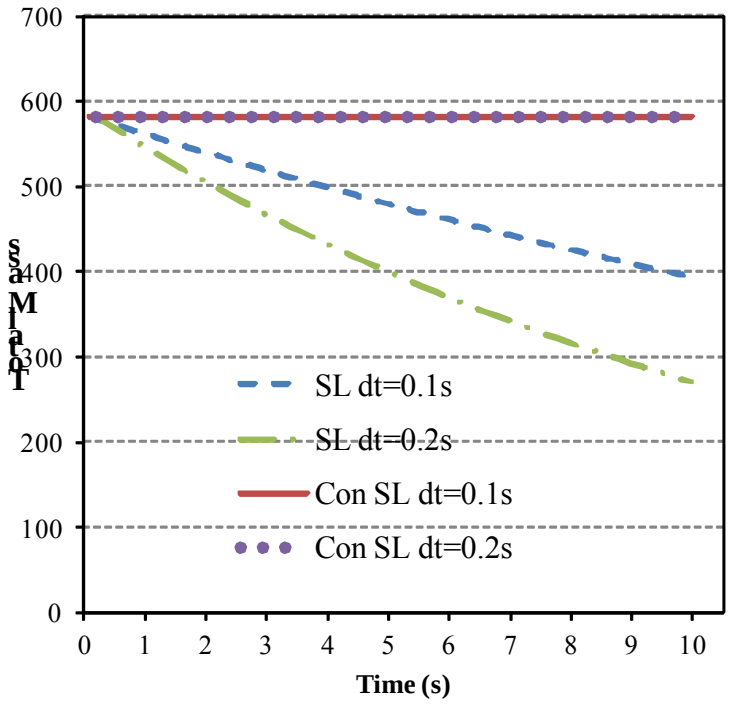

Figure 4. The total mass variation during one rotation as predicted by standard and conservative SL

3.2 Particle dispersion in a channel

Conservation of particle transport is important for use of FFD in predicting contaminant levels in buildings. This study used the case of particle dispersion in channel flow to test FFD performance with a conservative SL for preserving conservation in contaminant transport. FFD uses the Eulerian approach for particle transport, which is suitable only for particles with a small Stokes number; therefore, the reference data selected for this study were the data for hollow glass particles with St = 0.055 from the experiment by Snyder and Lumley (1971). As shown in Figure 5, the airflow velocity was 6.55 m/s through a channel with dimensions of 0.2m × 0.2m × 4m, and the corresponding Re was 1.3×10^5. The particles were injected at the center of the channel inlet with an assumed release rate of 10000 particles per second, and then dispersed in the channel. Our simulation used a grid size of 20 × 20 × 60, and time step size of 0.05 s with corresponding maximum CFL number of 4.5.The flow rate of the particles at the channel outlet was calculated in order to examine the conservation for particle transport. Meanwhile, the mean square displacement of particles was computed in order to evaluate FFD performance with a conservative SL for predicting particle dispersion. Since the Eulerian approach for particle transport was used, the mean square displacement d was defined as:

$$d = \frac{\int_{d\Omega} C(A) r^2(A) dA}{\int_{d\Omega} C(A) dA}, \tag{16}$$

where C(A) is the particle concentration at a location A, r (A) the distance to the centerline of the channel, and $d\Omega$ the cross-sectional area of the channel.

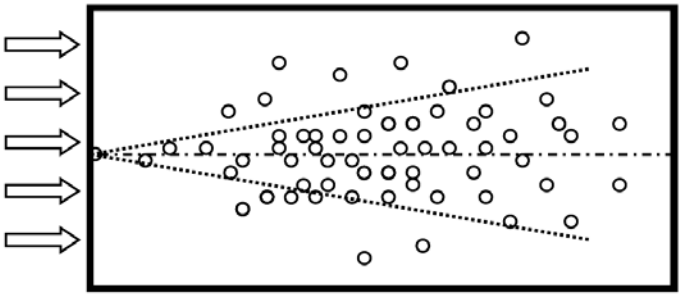

Figure 5. Schematic of particle dispersion in the channel

Since the FFD simulation did not use a turbulence model, it was difficult to obtain an accurate prediction of the particle dispersion caused by turbulent diffusion. To account for the turbulent diffusion, this study applied the effective particle diffusivity that was calculated using the turbulent viscosity measured in the experiment and the turbulent Schmidt number. In this case, the measured turbulent viscosity was $\nu_T = 5.0\times10^4$ m^2/s (Snyder and Lumley,1971) and assumped turbulent Schimidt number of 0.75 (Tominaga and Stathopoulos, 2007). However, due to the numerical diffusion existed in FFD simulations, the predicted particle diffusion by FFD did not agree very well with the experimental observation, as shown in Figure 6. When the effective particle diffusivity was adjusted to $k_c=2.8\times10^4$ m^2/s, FFD with the standard SL was able to predict the general trend of particle dispersion with good accuracy. FFD with the conservative SL can predict the same particle dispersion as FFD with the standard SL. Thus, use of the conservative SL rather than the standard SL has a negligible impact on the accuracy of the particle dispersion.

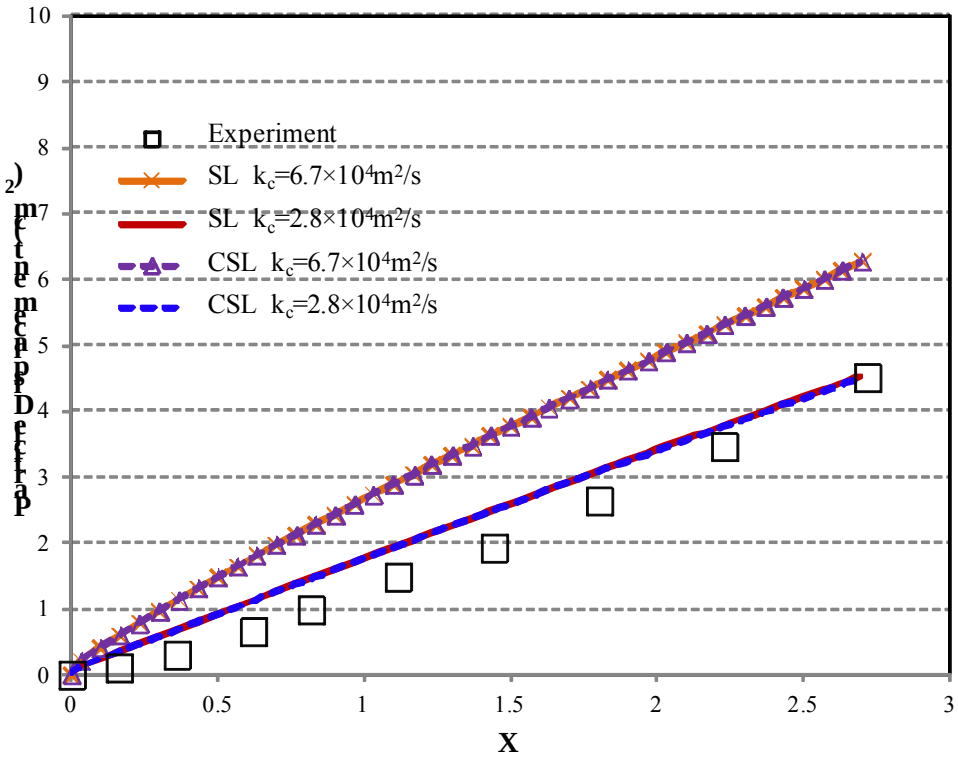

Figure 6. The mean square displacement of particles in the channel

To examine conservation of particle transport, Table 1 summarizes the particle flow rate at the inlet and outlet of the channel. FFD with both the standard and conservative SL can predict the conservative mass flow rate for particles at the channel outlet when the viscosity is low, as air viscosity $\nu=1.5 \times 10^{-5}$ m^2/s in this case. Because FFD performs only laminar simulation, the flow field predicted by FFD can be regarded as inviscid at such a low viscosity, leading to prediction of the pathline as straight-line in this case. The estimated backward trajectory in the standard SL can then be very accurate, so that particle transport becomes conservative in the advection process. At the same time, the viscous effect of the side wall would become significant with increased viscosity, forming a pathline with curvature. The standard SL would then be non-conservative because of the error in predicting the backward trajectory. Thus, as shown in Table 1, FFD with the standard SL cannot predict the correct mass flow rate for particles at the outlet with $\nu=1.5 \times 10^{-4}$ m^2/s and $\nu=1.5 \times 10^{-3}$ m^2/s. However, with the post correction for restoring global conservation, FFD with the conservative SL can obtain a correct prediction.

Table 1 Flow rate of particles at the channel inlet and outlet for flows with different viscosities

	Inlet (1/s)	Outlet (1/s)		
		$\nu=1.5 \times 10^{-5}$ m^2/s	$\nu=1.5 \times 10^{-4}$ m^2/s	$\nu=1.5 \times 10^{-3}$ m^2/s
Standard SL	1.0×10^4	1.01×10^4	1.08×10^4	1.30×10^4
Conservative SL	1.0×10^4	1.0×10^4	1.0×10^4	1.0×10^4

3.3 Mixed ventilation in an empty chamber

Correctly predicting conservative energy transport between the air and wall is very important for studies of buildings. This investigation used mixed ventilation in an empty chamber to test the performance of FFD with the conservative SL. The mixed ventilation case is based on an experimental study conducted by Blay et al. (1993). As shown in Figure 7, the experiment used a chamber with dimensions of 1.04m × 1.04m × 0.7m, and measurements of air velocity were conducted at the center plane. The inlet and outlet heights were 0.018 m and 0.024 m, respectively. Cool air with a temperature of 15 ^oC was supplied with a velocity of 0.57 m/s. The surrounding walls and the ceiling were also at a temperature of 15 ^oC, but the bottom wall was heated to a constant temperature of 35^oC. The flow motion was a result of the interaction of both the inertia and buoyancy forces. This study used a grid size of 20 × 30 × 15 and time step size of 0.1s, with corresponding maximum CFL number of 2.1, to simulate the airflow motion and energy transport in the chamber.

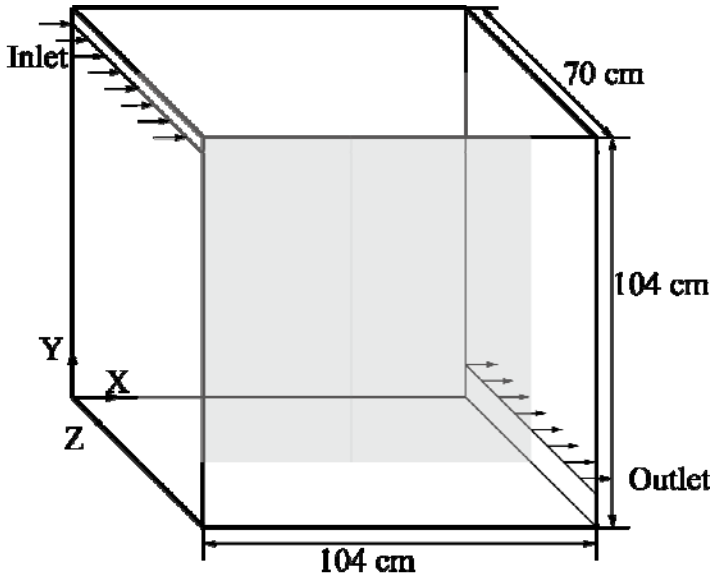

Figure 7. Schematic of mixed convection in a chamber with a heated floor

This study first examined the energy balance in the chamber. Through the transfer of energy from the hot surface of the chamber to the air, the cool air supplied to the chamber was heated and then exhausted at the outlet at a higher temperature. The energy transfer process for the air can be expressed by the following equation:

$$\frac{dQ_{air}}{dt} = q_{in} - q_{out} + q_{wall}, \tag{19}$$

where Q_{air} is the total energy of the air in the chamber, q_{in} the energy flow into the chamber at the inlet, q_{out} the energy flow out of the chamber at the outlet, and q_{wall} the energy transferred from the wall surfaces to the air. When a steady state was reached, the sum of the right-hand side of equation (19) should be zero if the energy conservation has been satisfied. To evaluate the conservativeness of the standard and conservative SL, this study defined the energy conservation error (ECR) as:

$$ECR = \frac{\left|q_{in} - q_{out} + q_{wall}\right|}{q_{wall}} \times 100\%, \tag{20}$$

which is the ratio of energy surplus/deficit in the air and energy transfer through the wall. Table 2 summarizes the energy flow in the chamber. FFD with the standard SL could not achieve conservative energy transfer; it predicts 56% more energy gain in the air than the energy transferred though the walls. At the same time, FFD with the conservative SL predicted the energy balance much more accurately, with an error of only 4.5%. This small error was caused primarily by temperature fluctuation in the domain. Because the buoyancy and inertial forces interacted strongly in this case, causing unstable airflow in the chamber, the temperature field showed small fluctuations even when a steady state was reached.

Table 2 The energy flow rate in the chamber

	q_{in} (W)	q_{out} (W)	q_{wall} (W)	ECR (%)
Standard SL	205.92	239.38	21.36	56.7
Conservative SL	205.92	233.12	26.04	4.5

Figure 8 presents the vertical and horizontal temperature profiles at cross sections X=0.52m and Y=0.5m, respectively. A comparison of the simulation results with the experimental data shows that FFD predicts similar temperature profiles with the standard and conservative SL. Both results are in good agreement with the experimental data, although the FFD simulation did not use a turbulence model. Because FFD with the standard SL predicted a higher energy gain in the air than the energy transferred through the walls, the post correction in the conservative SL subtracted the extra energy gain from the air; thus, FFD with the conservative SL predicted a slightly lower temperature than FFD with the standard SL in the vertical temperature profile at X=0.52m. However, because of the coupling between the energy and momentum equations, a change in the temperature field would cause variation in the velocity field and ultimately influence the temperature distribution. Thus, it is possible that the temperature predicted by FFD with the conservative SL would be higher than that predicted by FFD with the standard SL at some locations, as shown by the temperature profiles at Y=0.52m.

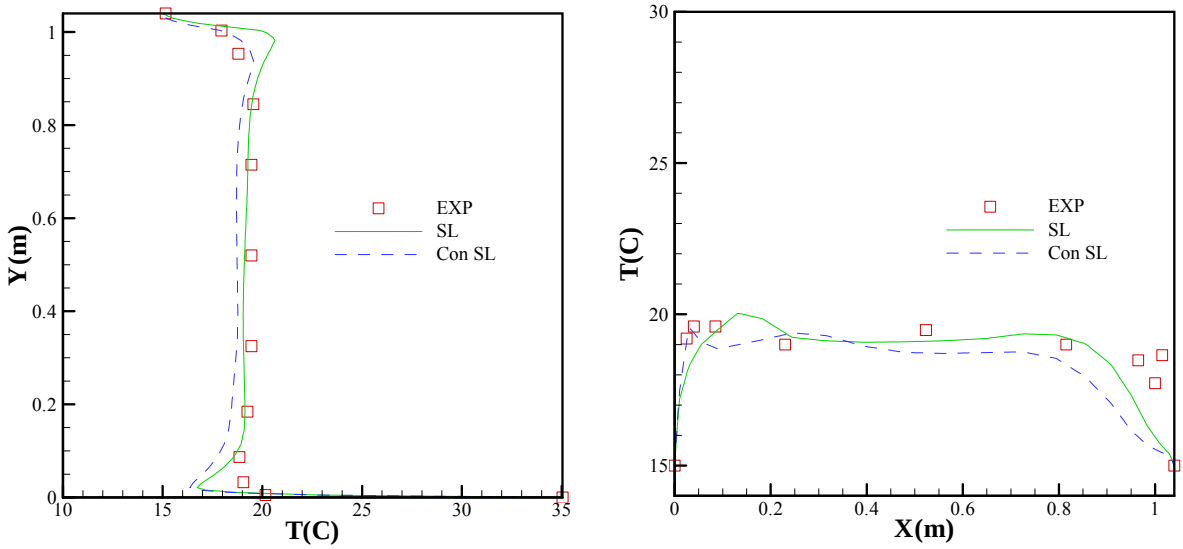

Figure 8. Comparison of temperature profiles at X=0.52m and Y=0.52m

3.4 Displacement ventilation in an occupied office

This study further applied FFD with the conservative SL to the simulation of indoor airflow in an occupied office space with displacement ventilation (Yuan et al. 1999), as shown in Figure 9. The office was simulated by an experimental chamber of 5.16m × 3.65m × 2.43m with a displacement diffuser on the side wall supplying air with a ventilation rate of 4 air changes per hour, or 183.1 m^3/h. The supply air temperature was 17.0^{o}C. The air was exhausted through an outlet located in the center of the ceiling. Because of the strong heat sources, such as the dummy occupants and computers, thermal stratification formed in the office space. In addition, a tracer gas with an injection rate of 40ml/h was released toward the two occupants to simulate contaminant transmission. The experiment measured the air temperature, air velocity, and tracer-gas concentration along nine vertical poles distributed in the streamwise center plane (P1–P5) and the cross-sectional center plane (P6-P9), as shown in Figure 9. This study used a grid size of 25 × 18 × 16 and time step size of 1.0s for FFD simulation of the room airflow, and the maximum CFL number in the simulation was 3.6.

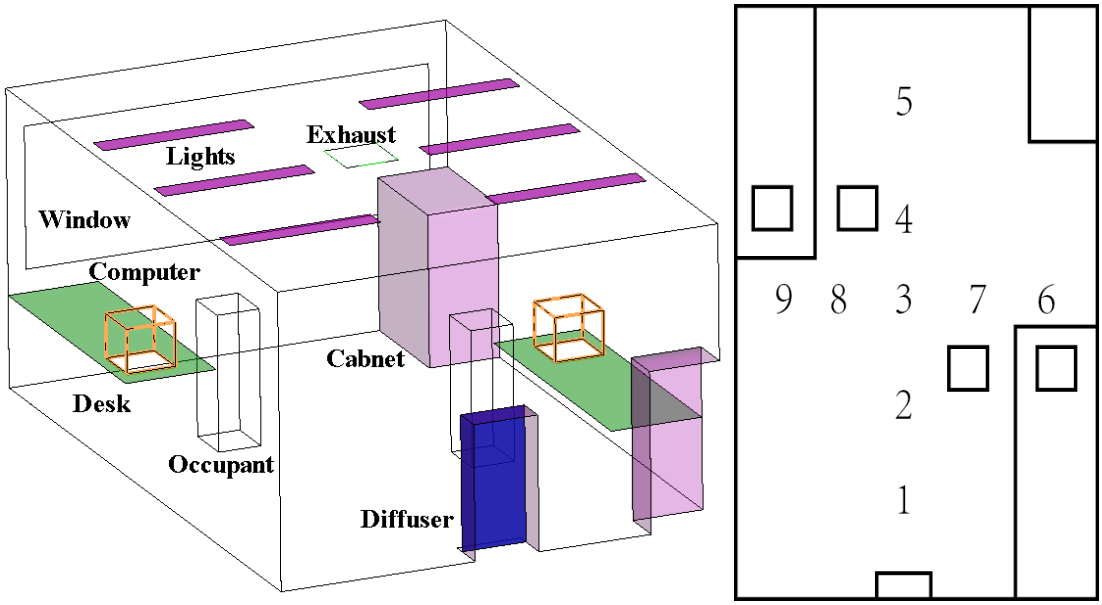

Figure 9. Schematic of displacement ventilation in the office space and measurement locations

Table 3 summarizes the energy balance in the office. With the standard SL, FFD cannot achieve energy conservation, with an 80% energy surplus in the air. In contrast, FFD with the conservative SL reduces the energy imbalance significantly, with an surplus of 5%. As stated in the third case, this small error may have been caused by a fluctuation in the temperature field.

Table 3 The energy flow rates in the office

	q_{in} (W)	q_{out} (W)	q_{wall} (W)	Error (%)
Standard SL	1015.56	1649.7	352.17	80.1
Conservative SL	1015.56	1626.3	581.49	5.0

Table 4 compares the injection rate of the tracer gas in the room and the flow rate of the tracer gas exiting through the outlet. FFD with the conservative SL predicted a low imbalance ratio of 0.7%, compared with 35.4% as predicted by FFD with the standard SL. Thus, the conservative SL can improve FFD performance for predicting conservative species concentration transport in indoor airflow simulations.

Table 4 The tracer-gas flow rates in the office

	Tracer-gas injection (ml/h)	Tracer gas exiting through the outlet (ml/h)	Error (%)
Standard SL	80	108.3	35.4
Conservative SL	80	79.4	0.7

Figure 10 depicts the temperature profiles at the five measurement locations (PI-P5) for assessment of FFD performance in predicting energy conservation. Because the simulated temperature profiles agree well with the experiment data, FFD with both the standard and conservative SL can predict the thermal stratification in the room. Much like the mixed convection in the empty chamber discussed in Section 3.3, the office-space temperature simulated by FFD with the conservative SL is seen to be slightly lower than with the standard SL because of redistribution of the energy surplus in the temperature field.

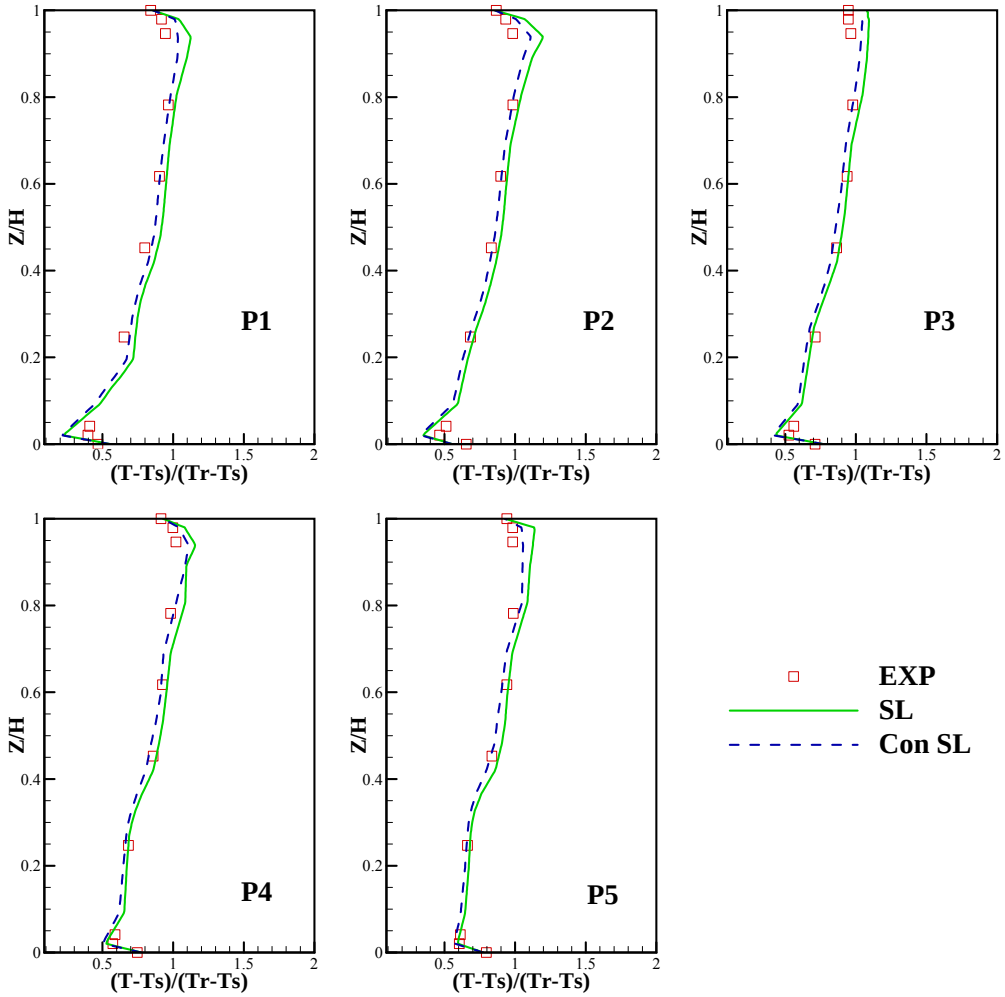

Figure 10. Comparison of air temperature profiles at positions P1 to P5.

This study further compared the simulated tracer-gas distributions with the measured data at positions P1 to P5, as shown in Figure 11. In comparison with the experimental data, the profiles simulated by FFD are of acceptable accuracy at P1, P2, and P3, but with a large discrepancy at the ceiling level at P4 and P5. However, FFD can still predict the primary characteristics of the tracer-gas distribution in the room, such as tracer-gas concentration stratification. In addition, FFD with the conservative SL performed as well as FFD with standard SL. This further confirms that the conservative SL would have a negligible impact on the scalar field distribution. Thus, FFD with the conservative SL can ensure conservation of the tracer-gas concentration.

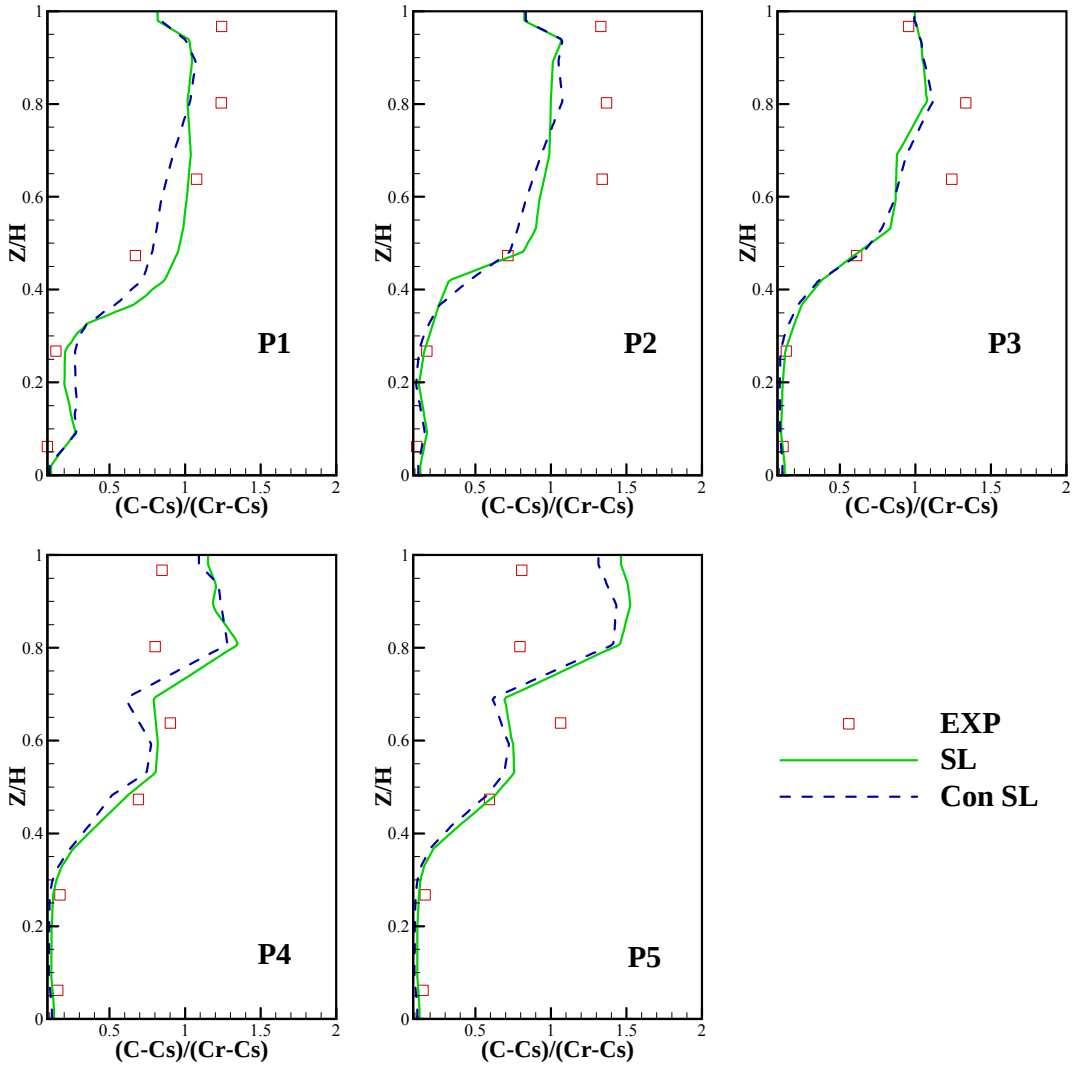

Figure 11. Comparison of tracer-gas concentration profiles at positions P1-P5.

4. Conclusions

This study proposed a conservative semi-Lagrangian scheme that applied a new mass-fixing method beyond the standard semi-Lagrangian scheme to restore the conservative advection. The new scheme was then implemented in FFD to achieve conservation in airflow simulations. The impact of the conservative semi-Lagrangian scheme on improving the accuracy and conservativeness of FFD simulations was assessed by applying it to several indoor airflows with experimental data from the literature.

Through the construction of redistribution weights depending on the difference between the standard semi-Lagrangian scheme solution and the local extreme value at the departure point, the explicit post correction was combined with the standard semi-Lagrangian scheme to restore global conservation during the advection process. The proposed method was able to achieve continuous correction, reduce the correction to the smooth field, and produce a monotonic solution. The effectiveness of the conservative semi-Lagrangian scheme was validated with several test cases, and the results show that the proposed scheme is indeed conservative with negligible impact on the accuracy of the standard solutions.

The conservative semi-Lagrangian scheme was further implemented in FFD to solve the advection equations for scalar transport equations. The improved FFD was tested in several indoor airflow cases with energy and species transport. The results showed that FFD with the conservative semi-Lagrangian scheme can effectively enforce the energy and species conservation for indoor airflow simulations. The conservative semi-Lagrangian scheme had a negligible influence on the airflow distributions, and it predicted similar temperature and species concentration profiles as did FFD with the standard semi-Lagrangian scheme.

References

Bermejo, R. and A. Staniforth (1992). "The conversion of semi-Lagrangian advection schemes to quasi-monotone schemes." *Monthly Weather Review,* Vol. 120 No.11,pp. 2622-2632.

Blay, D., S. Mergui and C. Niculae (1993). "Confined turbulent mixed convection in the presence of a horizontal buoyant wall jet." *ASME-Publications-HTD,* Vol. 213 pp. 65-65.

Chorin, A. J. (1967). "A numerical method for solving incompressible viscous flow problems." *Journal of computational physics,* Vol. 2 No.1,pp. 12-26.

Ferziger, J. H. and M. Perić (1999). *Computational methods for fluid dynamics*.Springer, New York.

Jin, M., W. Zuo and Q. Chen (2012). "Improvements of fast fluid dynamics for simulating air flow in buildings." *Numerical Heat Transfer, Part B: Fundamentals,* Vol. 62 No.6,pp. 419-438.

Jin, M., W. Zuo, and Q. Chen (2013). "Simulating Natural Ventilation in and Around Buildings by Fast Fluid Dynamics." *Numerical Heat Transfer, Part A*: *Applications,* Vol. 64, No. 4, pp: 273-289.

Kaas, E. (2008). "A simple and efficient locally mass conserving semi‐Lagrangian transport scheme." *Tellus A,* Vol. 60 No.2,pp. 305-320.

Lauritzen, P. H., R. D. Nair and P. A. Ullrich (2010). "A conservative semi-Lagrangian multi-tracer transport scheme (CSLAM) on the cubed-sphere grid." *Journal of Computational Physics,* Vol. 229 No.5,pp. 1401-1424.

Lentine, M., J. T. Grétarsson and R. Fedkiw (2011). "An unconditionally stable fully conservative semi-Lagrangian method." *Journal of Computational Physics,* Vol. 230 No.8,pp. 2857-2879.

Priestley, A. (1993). "A quasi-conservative version of the semi-Lagrangian advection scheme." *Monthly Weather Review,* Vol. 121 No.2,pp. 621-629.

Rancic, M. (1995). "An efficient, conservative, monotonic remapping for semi-Lagrangian transport algorithms." *Monthly weather review,* Vol. 123 No.4,pp. 1213-1217.

Rančic, M. (1992). "Semi-Lagrangian piecewise biparabolic scheme for two-dimensional horizontal advection of a passive scalar." *Monthly weather review,* Vol. 120 No.7,pp. 1394-1406.

René Laprise, J. and A. Plante (1995). "A class of semi-lagrangian integrated-mass (SLM) numerical transport algorithms." *Monthly Weather Review,* Vol. 123 No.2,pp. 553-565.

Robert, A. (1981). "A stable numerical integration scheme for the primitive meteorological equations." *Atmosphere-Ocean,* Vol. 19 No.1,pp. 35-46.

Snyder, W. and J. Lumley (1971). "Some measurements of particle velocity autocorrelation functions in a turbulent flow." *Journal of Fluid Mechanics,* Vol. 48 pp. 41-71.

Stam, J. (1999). "Stable fluids". *Proceedings of the 26th annual conference on Computer graphics and interactive techniques*, ACM Press/Addison-Wesley Publishing Co.

Staniforth, A. and J. Côté (1991). "Semi-Lagrangian integration schemes for atmospheric models-a review." *Monthly Weather Review,* Vol. 119 No.9,pp. 2206-2223.

Yoshihide, T., and T. Stathopoulos (2007). "Turbulent Schmidt numbers for CFD analysis with various types of flowfield." *Atmospheric Environment* , Vol.41, No. 37, pp. 8091-8099.

Yuan, X., Q. Chen, L. Glicksman, Y. Hu and X. Yang (1999). "Measurements and computations of room airflow with displacement ventilation." *ASHRAE Transactions,* Vol. 105 No.1,pp. 340-352.

Zalesak, S. T. (1979). "Fully multidimensional flux-corrected transport algorithms for fluids." *Journal of computational physics,* Vol. 31 No.3,pp. 335-362.

Zerroukat, M. (2010). "A simple mass conserving semi-Lagrangian scheme for transport problems." *Journal of Computational Physics,* Vol. 229 No.24,pp. 9011-9019.

Zerroukat, M., N. Wood and A. Staniforth (2002). "SLICE: A Semi‐Lagrangian Inherently Conserving and Efficient scheme for transport problems." *Quarterly Journal of the Royal Meteorological Society,* Vol. 128 No.586,pp. 2801-2820.

Zerroukat, M., N. Wood and A. Staniforth (2005). "A monotonic and positive–definite filter for a Semi-Lagrangian Inherently Conserving and Efficient (SLICE) scheme." *Quarterly Journal of the Royal Meteorological Society,* Vol. 131 No.611,pp. 2923-2936.

Zuo, W. and Q. Chen (2009). "Real‐time or faster‐than‐real‐time simulation of airflow in buildings." *Indoor air,* Vol. 19 No.1,pp. 33-44.

Zuo, W. and Q. Chen (2010). "Fast and informative flow simulations in a building by using fast fluid dynamics model on graphics processing unit." *Building and environment,* Vol. 45 No.3,pp. 747-757.

Zuo, W., J. Hu and Q. Chen (2010). "Improvements in FFD modeling by using different numerical schemes." *Numerical Heat Transfer, Part B: Fundamentals,* Vol. 58 No.1,pp. 1-16.